Comprehensive Exam

Khalid Omer, PhD Student

1 Introduction

Traditional cameras measure the irradiance produced by the emission, scatter, and reflection of a scene. However, the traditional method of imaging does not provide information regarding the polarization state of the incoming light. Polarimeters measure the polarization state of the light by utilizing optical elements that either filter or perturb the incoming field which and then analyzed. Imaging polarimeters are devices that use a focal plane array as the analyzing unit and form images to visualize the polarization of a scene. In this paper, a micro-grid imaging polarimeter shall be described. In particular, a linear Stokes micro-grid imaging polarimeter from LUCID Vision Labs [1]. This camera uses a Sony IMX250MZR CMOS focal plane array (FPA) with a wire-grid polarizer array over the top of the sensor.

In OPTI 501, light is described as a transverse electromagnetic wave characterized by the waves' amplitude, phase, and oscillation direction. The electric and magnetic field oscillates in the direction perpendicular to travel. Along with being perpendicular to the travel direction, both the electric and magnetic field are perpendicular to each other creating a right-handed coordinate system. In OPTI 505, the direction of oscillation defines the polarization state. By convention, the electric field direction is used. The electric field of a monochromatic wave as seen in OPTI 501 and 505 is:

$$\mathcal{E}(\mathbf{r},t) = \mathrm{Re}\left[\mathbf{E}e^{i\left(\frac{2\pi}{\lambda}\mathbf{k}\cdot\mathbf{r}-\omega t-\phi_0\right)}\right] = \mathrm{Re}\left[\begin{pmatrix} E_x \\ E_y \\ E_z \end{pmatrix} e^{i\left(\frac{2\pi}{\lambda}\mathbf{k}\cdot\mathbf{r}-\omega t-\phi_0\right)}\right]. \tag{1}$$

Here $\mathcal{E}(\mathbf{r},t)$ is the spatio-temporal vector-valued electric field and λ is the wavelength. The magnitude and direction of oscillation of the electric field are determined by the complex-valued components of the polarization vector $\mathbf{E} = (E_x, E_y, E_z)$. The normalized wavevector $\mathbf{k} = (k_x, k_y, k_z)$ components are direction cosines and $\mathbf{r} = (x, y, z)$ is the position in space. The time is t in units of sec, ω is the angular frequency in rad/sec, and ϕ_0 is the phase offset in rad. The polarization vector can be expressed as magnitude and phase of each component $\mathbf{E} = [A_x e^{-i\phi_x}, A_y e^{-i\phi_y}, A_z e^{-i\phi_z}]$. For a transverse electromagnetic wave propagating along the z-axis $\mathbf{k} = (0, 0, 1)$, the electric field is restricted to the transverse x-y plane, *i.e.* only $[E_x, E_y]$ are non-zero. In this two-component form, the polarization vector is called the Jones vector. The motion of the electric field vector projected onto the transverse plane traces either: a circle, ellipse, or a line. For linear polarization states, the relative phase $\phi = \phi_y - \phi_x$ is zero or π. For circular polarization states $A_x = A_y$ and $\phi = \pm\pi/2$. The

Jones vector describes monochromatic light propagating in a single direction. There is no spectral, spatial, or temporal incoherence of this field.

When the electric field vector does not trace an elliptical shape in the transverse plane the light is not fully-polarized. For example, sunlight, lightbulbs, and flashlights are sources of unpolarized light. For incoherent and polychromatic light, Jones vectors are not a suitable method for describing polarization. In this scenario, the Stokes parameters describe unpolarized, partially-polarized, and polarized light; including for coherent and incoherent light sources [2]. Six polarized flux measurements with ideal polarizers define the four Stokes parameters

$$\mathbf{S} = \begin{pmatrix} P_H + P_V = P_{45} + P_{135} = P_R + P_L \\ P_H - P_V \\ P_{45} - P_{135} \\ P_R - P_L \end{pmatrix} = \begin{pmatrix} S_0 \\ S_1 \\ S_2 \\ S_3 \end{pmatrix}. \tag{2}$$

Here, $P_H - P_V$ is the difference between horizontal and vertical polarization flux measurements, $P_{45} - P_{135}$ is the difference between 45° and 135° measurements, and $P_R - P_L$ is the difference between right and left circular measurements. The four Stokes parameters form a non-orthogonal coordinate system and do not transform or rotate like vectors. Therefore, the Stokes parameters are not vectors but operate in terms of addition and multiplication in the same manner. For the camera detailed in this paper P_H, P_V, P_{45}, and P_{135} are measured for each waveband in RGB, totaling to 12 measured polarimetric values. Imaging polarimetry requires image fusion techniques to consolidate the polarimetric data into a format that can be processed and displayed in a traditional RGB display [2]. Below describes several imaging polarimetry methods to display polarimetric images shown in OPTI 586 as well as research methods [3].

The degree of linear polarization (DoLP) is the ratio of the linearly polarized irradiance (I_{pol}) to the total irradiance (S_0)

$$\text{DoLP} = \frac{\sqrt{{S_1}^2 + {S_2}^2}}{S_0} = \frac{I_{pol}}{S_0}, \tag{3}$$

where a $DoLP = 0$ implies no linear polarization, and a $DoLP = 1$ corresponds to fully linearly polarized. When imaging polarimetry, DoLP as calculated in Equation 3 is traditionally displayed as a monochromatic image. In Figure 1b, the DoLP of the red, green, and blue channels are calculated to form a polychromatic DoLP.

The angle of linear polarization (AoLP) is

$$\text{AoLP} = \frac{1}{2}\arctan 2\left(\frac{S_2}{S_1}\right), \tag{4}$$

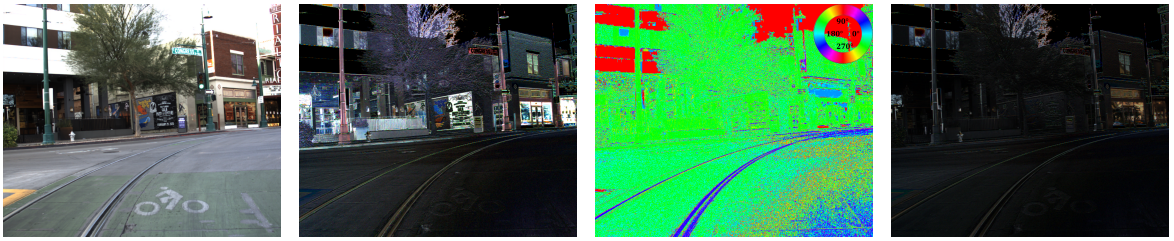

(a) RGB (b) DoLP (c) AoLP (d) I_{pol}

(e) Umov Fusion (f) Fusion (g) IHS

Figure 1: An example frame an imaging polarimeter: (a) RGB, (b) DoLP where dark objects have a high DoLP due to Umov's effect, (c) AoLP where metal streetcar railings and windows are prominent, (d) I_{pol} which has less chromatic features as compared to DoLP, (e) Umov's Fusion where a majority of the color information is retained with exceptions such as green metallic street lights, (f) Fusion where color information is lost but regions of low irradiance and high polarization are increased in contrast, and (g) IHS where more color information is preserved as compared to the green street light in Umov Fusion and regions of low irradiance and high polarization are increased in contrast.

where the AoLP is bounded between 0°and 180°. The AoLP, as calculated in Equation 4, uses a color map that takes a monochromatic AoLP image into an HSV format when imaging polarimetry; see Figure 1c.

The linear polarized irradiance I_{pol} is,

$$I_{pol} = S_0 \times \text{DoLP}. \tag{5}$$

Here a pixel-wise multiplication between the RGB image (S_0) and the polychromatic DoLP is computed. The RGB image range is 0-255 and DoLP range is 0-1; see Figure 1d for an I_{pol} image example.

The Umov Fusion adopts a portion of an image fusion technique for regions of low irradiance and high polarization

$$\text{Umov Fusion} = \max\{S_0, \text{DoLP}\}. \tag{6}$$

Here a pixel-wise operation between the RGB image (S_0) and the polychromatic DoLP replaces low contrast regions of an RGB image with polarimetric information. Dark regions of RGB images can be rich in polarimetric information due to Umov's effect, which describes an inverse relationship between albedo and degree of polarization. An example of Umov Fusion is given in Figure 1e.

Fusion transforms polarimetric data to the HSV colorspace by $\text{H} \rightarrow 2\text{AoLP}, \text{S} \rightarrow \text{DoLP}, \text{V} \rightarrow$ Umov Fusion.

An example fusion image is given in Figure 1f. Areas of low irradiance are enhanced by this fusion with polarimetric data. However objects do not retain their true color using the Fusion transform. To retain color information and add polarimetric information, panchromatic sharpening methods are adapted. [4] Panchromatic sharpening combines low-resolution color images with higher-resolution monochromatic images. Intensity-hue-saturation (IHS) is a panchromatic sharpening technique that retains the color of the low-resolution image by replacing the low-resolution brightness values with the higher-resolution monochromatic values. This method is adapted to polarization data by considering the RGB image as the low-resolution carrier and Umov Fusion as the higher-resolution image. First, the original RGB image is converted to an HSV format. Next, the brightness values are swapped with Umov Fusion $V \rightarrow \max\{S_0, \text{DoLP}\}$. Finally, the modified HSV image is then reverted to an RGB format. See Figure 1g for an example IHS image fusion.

2 Linear-Stokes Polarimeters

Polarizers are optical elements that transmit and block specific polarization states. The transmission of a polarizer is polarization-dependent. Linear polarizers are elements that transmit linearly polarized light that is aligned with the polarizer's transmission axis and blocks linearly polarized light orthogonal to this transmission axis. For example, unpolarized light incident onto an ideal horizontal linear polarizer will transmit horizontal light on the other side of the interface. The transmission is 0.5 since unpolarized light can be modeled as equal parts of two orthogonal polarization states. An ideal polarizer does not transmit light in the orthogonal polarization state. One of the methods to determine the performance of a polarizer is with the Extinction ration (ER), $ER = \frac{T_{max}}{T_{min}}$. The ER is the ratio between the maximum and minimum transmission of a polarizer. T_{max} is the transmission of light polarized along the transmission axis, while T_{min} is the transmission of light polarized orthogonal to the transmission axis. Types of polarizers include dichroic and wire-grid polarizers.

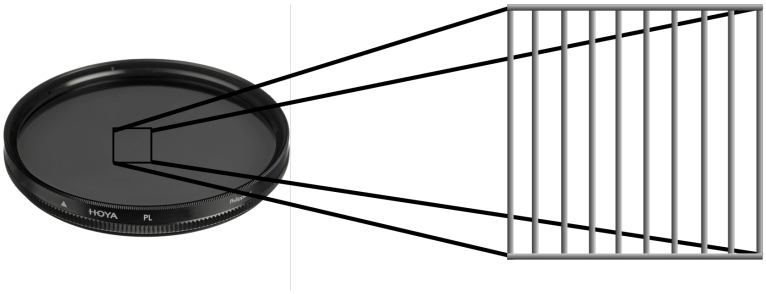

Figure 2: Image of a wire-grid polarizer [5]. The drawing on the polarizer shows the parallel structure of the metallic wires. Lithographic methods are used to create these polarizers that have sub-wavelength air spacing.

Dichoric polarizers contain differences in the transmission axis that result in diattenuation via propagation.

Linear dichroic polarizers are often used in conjunction with a quarter-wave plate to create circular polarizers. Sony uses wire-grid polarizers due to their small size, low cost, and ability work in a variety of environments. Wire-grid polarizers contain a parallel metallic wires with sub-wavelength spacing as depicted in Figure 2. The transmission axis for wire-grid polarizers is orthogonal to the grid of wires. The physics of wire-grid polarizers utilizes principles learned in OPTI 501 and OPTI 511R. When light polarized in the direction orthogonal to the transmission axis is incident to the polarizer, the electric field then generates a current along the direction of the wires [6]. This current results in an interaction between electrons and atoms within the metal and converts the field energy to heat. For the light along the transmission axis the interaction with the wire-grid is limited and does not generate a current that transfers the field energy to heat. This limitation is due to the lack of motion for electrons to move along the transmission axis.

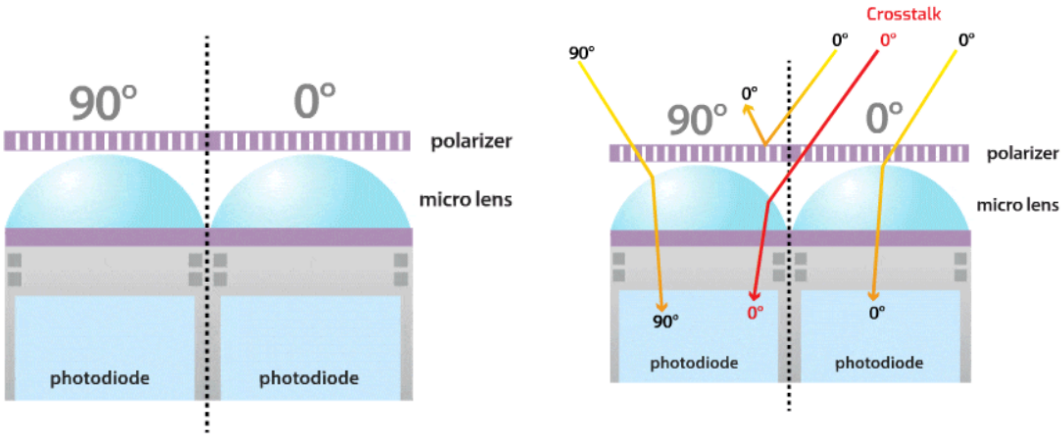

(a) 4D Sensor [1]

(b) Cross-talk [1]

Figure 3: (a) Diagram of 4D sensor design of their PolarCam linear-Stokes camera. Wire-grid polarizer array resides above the microlens array. (b) Rays depicting cross talk between polarizers as a result of the over the lens polarizers. Light polarized at 0°passes through the 0°polarizer that then passes through the lens directed towards the pixel measuring 90°.

Wire-grid polarizer arrays for linear-Stokes imaging contain a periodic set of four linear polarizers at 0, 45°, 90°, and 135° arranged in a 2×2 grid. The polarizers in the array have dimensions on the order of the pixel size. To increase collection efficiency, the design of these cameras utilizes microlens array to focus the beam into the collection region. Historically, there have been two forms of linear-Stokes imaging cameras geared towards consumers. The first iteration comes from 4D Technology, where the polarizer array resides above the microlens array as seen in Figure 3a. As was learned in OPTI 537, the light with energy $E = h\nu$ incident onto a reverse-biased semiconductor material (photodiode) is then converted into a measured electrical signal. However, the 4D PolarCam suffered from large amount of cross talk between pixels. Figure 3b shows cross talk between pixels with the microlens focusing the light by refraction. This concept was taught in OPTI 502

and is described by Snell's law $n_1 \sin(\theta_1) = n_2 \sin(\theta_2)$. Refraction occurs due to the index of refraction, n_1 and n_2, and the differences between the air and the material of the microlens array index which in most cases is either plastic or glass. Light with an incoming angle of θ_1 is then refracted to an angle θ_2, where both angles are measured normal to the surface.

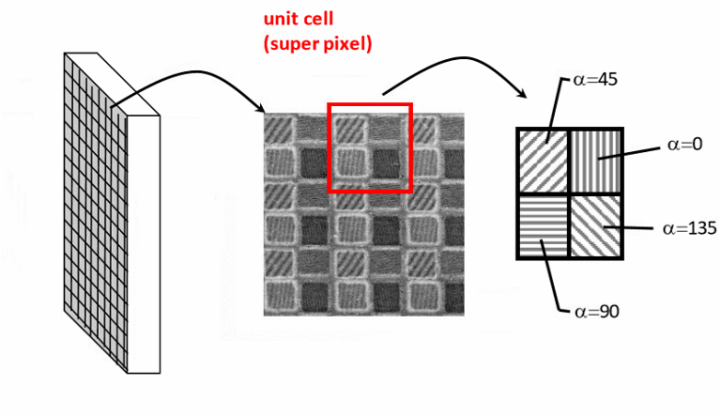

Figure 4: Diagram illustrating micro-polarizer array arrangement [7]. Polarizers are arranged to minimize the amount of cross-talk between orthogonal states.

One method used to limit the cross-talk is to place the polarizers in a pattern that limits the signal from an orthogonal state. Such a structure for the micro-polarizer array is shown in Figure 4. Orthogonal states typically have the largest contrast when looking at pixel values; see Figure 6a. These large differences in the pixel read out can result in blooming and various other forms of electronic noise. Additionally, By creating this pattern, any cross talk due to adjacent polarizers as seen in Figure 3b would be reduced by half by having either the 45° or 135° polarizers in place of the 0° polarizer.

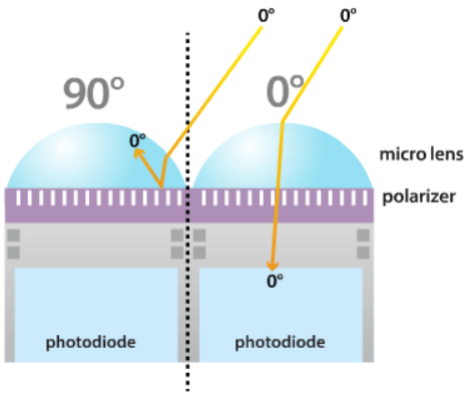

Figure 5: Illustration of Sony sensor design used in the Lucid Lab's Triton 5MP Polarization camera [1]. The micro-grid polarizer array resides on the surface of the camera sensor.

The Sony design in Figure 5 furthered the development of the sensor design by adjusting the position of

the polarizer to be directly above the photodiode array. As seen in the figure, the chances of cross talk are reduced due to the 0° polarizer being on-chip.

The Sony and 4D Technology sensor designs suffer from mosaicing due to the gridding of polarizers. Mosaicing is a common issue with Bayer filters. Bayer filters are overlayed image sensors and processed to form colored images with post-processing algorithms to demosaic an image. Here, the micro-polarizer array can be viewed as a Bayer filter for polarization. Techniques such as bilinear interpolation and gradient-based methods are used to demosaic an image. These methods have been incorporated into demosaicing polarimetric images. The method used by 4D and Sony incorporate a method detailed by S. Tyo, et.al [8]. This method reconstructs spatially band-limited polarization images by using a linear system framework. This method utilizes mathematical techniques learned in OPTI 505, 512L, and 536. Details regarding this method can be found in Section 4.

3 Camera Properties

The linear-Stokes camera uses a fixed focal length lens to image scenes. The details regarding the system properties of the camera are provided in the table below:

System Properties	
$F/\#$	2-16
FOV	$41.2° \times 31.02°$
Focal Length f	12 mm
Pixel Pitch	3.45 $\mu m(H) \times 3.45$ $\mu m(V)$
ER(R,620nm)	316.91
ER(G,540nm)	472.94
ER(B,470nm)	637.2

Table 1: Lucid Lab's Triton 5MP Polarization camera

Here, $F/\# = f/D_{EP}$ is the ratio of the focal length to the diameter of the entrance pupil. The entrance pupil is the image of the stop in object space that defines the cone of light entering the optical system. The f-number is an infinite-conjugate quantity. For finite conjugates, the working f-number $F/\#_w = (1-m)F/\#$ [9]. The variable f-number, known as f-stops, are due to changes in the entrance pupil size, and not directly related to the working f-number. These f-stops are marked in increments of $\sqrt{2}$. A $\sqrt{2}$ increase in the f-number with fixed focal length relates to a factor of 2 area decrease. A decrease in the area then relates to a decrease in the amount of light that passes through the optical system (since it is the entrance pupil). Therefore, for well-lit scenes, the f-number was set to a higher value to avoid over saturation in the camera. For areas with limited lighting, the f-number was adjusted to a lower value to increase the amount of light. Using the $F/\#$

and focal length one can then calculate the entrance pupil. In OPTI 502 the term "fast lens" and "slow lens" refers to a low and high f-number; respectively [9].

Additionally, the FOV of the lens provides insight on the size of the light that reaches the detector in the horizontal and vertical direction.

$$h' = f \tan\left(\frac{FOV}{2}\right) \tag{7}$$

Here, h' is the maximum size of an image from the z-axis produced by the lens and is determined by the chief ray of a distant object. For FOV = $41.2° \times 31.02°$, the maximum image extent is $9.02mm \times 6.66mm$ across the entire sensor. This relates to a diagonal length of 11.1 mm which matches the size of the standard 2/3" sensor format.

The ER as discussed in 2 provides quantities performance of polarizer detection. The signal detected with the microgrid polarizers depends on the pixel channel (RGB) and the wavelength of the incoming light. Table 1 shows the maximum ER for a given color channel and wavelength with $ER(R, 620\ nm) = 316.91$, $ER(G, 540\ nm) = 472.94$, $ER(R, 470\ nm) = 637.2$. The wavelength that maximizes the ER corresponds to the color of the channel used for detection. The ER for the blue channel has the largest value compared to the red and green channels. Although the data is not provided, the wire-grid polarizers is likely fabricated for maximum transmission in the blue waveband and would explain the fall-off for the red and green waveband.

4 Demosaicing: Linear System Framework

Measurements from the linear-Stokes camera result in a mosaic due to the polarization measurements being made from different locations on the FPA. Although still a linear process, the polarization-dependent point spread function (PSF) for the imaging system is not shift-invariant across the image plane. The image formed on the detector is expressed as

$$g(n, m) = \mathbf{S_A}(n, m)^\intercal \cdot \mathbf{S_f}(n, m), \tag{8}$$

where m and n are the pixel positions, $g(n, m)$ is the noise-free image irradiance, S_A is the analyzer vector, and $\mathbf{S_f} = (s_0(n, m), s_1(n, m), s_2(n, m), s_3(n, m))$ is the Stokes vector of the light incident on a given pixel. The analyzer vector,

$$\mathbf{S}_A(n, m) = \frac{1}{2} \begin{bmatrix} 1 \\ \frac{1}{2}(\cos(m\pi) + \cos(n\pi)) \\ \frac{1}{2}(\cos(m\pi) - \cos(n\pi)) \\ 0 \end{bmatrix} \tag{9}$$

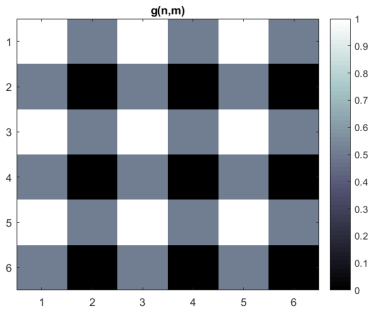

(a) Mosaic Image $g(n,m)$

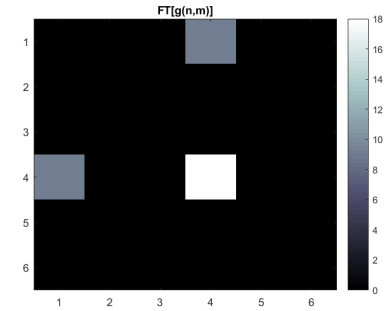

(b) Fourier Transform of Mosaic Image $\tilde{g}(n,m)$

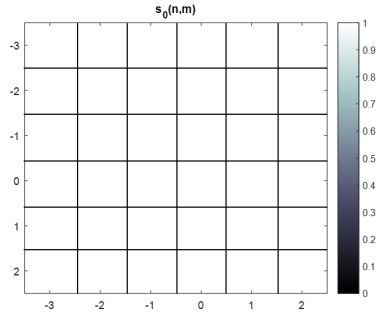

(c) Reconstructed Image $s_{0,recon}(n,m)$

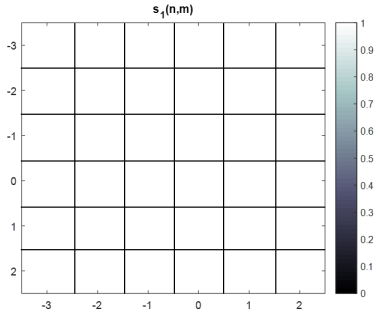

(d) Reconstructed Image $s_{1,recon}(n,m)$

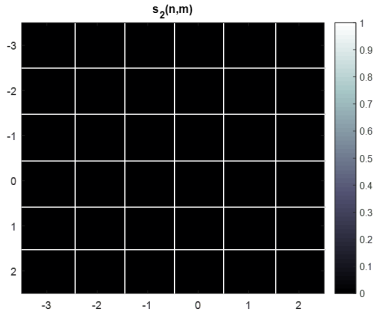

(e) Reconstructed Image $s_{2,recon}(n,m)$

Figure 6: (a) $g(n,m)$ simulates mosaicing on a 6×6 FPA. Input signal of $S_f(n,m) = (1,1,0,0)$ for all pixel position demonstrates the varying flux measurements between polarizers. When $n = odd$ and $m = odd$ the horizontal polarizer completely transmits the input. The polarizer is vertically polarized when $n = even$ and $m = even$ and does not transmit the input. (b) Image of the Fourier transform of a band-limited mosaic image $\mathcal{F}\{\text{g(n,m)}\}$. Signal being carried at $\xi = 0, \eta = 0$ corresponds to $\tilde{s}_0(\xi,\eta)$. Due to the wrapping in Fourier space from the DFT, $\xi = \frac{1}{2}, \eta = 0$, carries the signal for $\widetilde{s}_1\left(\xi - \frac{1}{2}, \eta\right) + \widetilde{s}_2\left(\xi - \frac{1}{2}, \eta\right)$. Lastly, $\xi = 0, \eta = \frac{1}{2}$ represents the signal at $\widetilde{s}_1\left(\xi, \eta - \frac{1}{2}\right) + \widetilde{s}_2\left(\xi, \eta - \frac{1}{2}\right)$. (c-e) Reconstructed images of the $s_0(n.m), s_1(n.m), s_2(n.m)$ using the three distinct values in $\tilde{g}(\xi,\eta)$ as low-pass filters.

describes the micro-grid polarizer array across the entire image plane. The analyzer vector used follows the geometry of micro-grid polarizers as seen in Figure 4. The image on the detector can then be expressed as

$$g(n,m) = s_0(n,m) + \frac{1}{2}\cos(m\pi)\left[s_1(n,m) + s_2(n,m)\right] + \frac{1}{2}\cos(n\pi)\left[s_1(n,m) - s_2(n,m)\right] \quad . \tag{10}$$

An example input if $\mathbf{S_f}(n,m) = (1,1,0,0)$ is used to demonstrate the mosaicing of the linear-Stokes polarimeter shown in Figure 6. The horizontally polarized light results in a mosaiced image where the horizontal polarizer fully transmits, the vertical polarizer fully absorbs, and the 45° and 135° polarizers transmit half of the light. To demosaic the image, Sony uses methods detailed by S. Tyo, et. al [8] that reconstructs the scene in the frequency domain. The Fourier transform takes the spatial varying image into the spatial frequency domain.

The Fourier transform of $g(n,m)$ is

$$\tilde{g}(\xi,\eta) = \tilde{s}_0(\xi,\eta) + \frac{1}{4}\left[\widetilde{s}_1\left(\xi-\frac{1}{2},\eta\right)+\widetilde{s}_2\left(\xi-\frac{1}{2},\eta\right)\right]+\frac{1}{4}\left[\widetilde{s}_1\left(\xi,\eta-\frac{1}{2}\right)-\widetilde{s}_2\left(\xi,\eta-\frac{1}{2}\right)\right] \quad . \tag{11}$$

Here, ξ and η are the horizontal and vertical spatial frequencies $\frac{cycles}{pixel}$, respectively. The tildes above the variables then imply the Fourier transform of the spatial variable. Interpretation of the equation suggest a signal from s_0 centered at the origin of Fourier space with side lobes located at $\xi = \frac{1}{2}$ representing $s_1(n,m) + s_2(n,m)$ and $\eta = \frac{1}{2}$ for $s_1(n,m) - s_2(n,m)$. Perfect reconstruction results when the signals is band limited. A band limited signal has finite extent in the Fourier domain. Optical systems such as cameras have finite sized apertures that result in band limited images. A non-band limited example includes images of distant stars that are approximated as point delta sources that when viewed in the Fourier domain are constant valued. For the signal in Figure 6a, this results in three distinct values in Fourier domain as seen in figure 6b. These distinct values correspond to the two lobes and a DC value in Equation 11. The central band limited region in the Fourier domain is used reconstruct the term s_0 by filtering the central value across the Fourier transformed image through multiplication, $s_{0,recon}(n,m) = \mathcal{F}^{-1}\{\tilde{g}(\xi,\eta)I_{LP}\}$. Here, I_{LP} is a low-pass filter generated with the central value corresponding to $\tilde{s}_0(\xi,\eta)$. Furthermore, s_1 and s_2 reconstruction occurs by low-pass filtering with the terms in the Fourier domain representing $s_1 + s_2$ and $s_1 - s_2$. Once processed, the reconstructed $s_{0,recon}$,$s_{1,recon}$, and $s_{2,recon}$ have the same dimensionality as the original image; see Figure 6c-e.

References

[1] Beyond conventional imaging: Sony's polarized sensor. *LUCID Vision Labs*.

[2] Russell A Chipman, Wai Sze Tiffany Lam, and Garam Young. *Polarized Light and Optical Systems*. CRC Press, 2018.

[3] Khalid Omer, Russell Chipman, and Meredith Kupinski. Road scene object detection using pre-trained RGB neural networks on linear Stokes images. In *Polarization: Measurement, Analysis, and Remote Sensing XIV*, volume 11412, pages 15 – 29. International Society for Optics and Photonics, SPIE, 2020.

[4] C. Pohl and J. L. Van Genderen. Review article multisensor image fusion in remote sensing: Concepts, methods and applications. *International Journal of Remote Sensing*, 19(5):823–854, 1998.

[5] Hoya 67mm linear polarizer filter. *B&H*.

[6] E. Hecht. *Optics*. Pearson education. Addison-Wesley, 2002.

[7] Neal Brock, Bradley Kimbrough, and James Millerd. A pixelated polarizer-based camera for instantaneous interferometric measurements. *Proceedings of SPIE - The International Society for Optical Engineering*, 09 2011.

[8] J. Scott Tyo, Charles F. LaCasse, and Bradley M. Ratliff. Total elimination of sampling errors in polarization imagery obtained with integrated microgrid polarimeters. *Opt. Lett.*, 34(20):3187–3189, Oct 2009.

[9] J.E. Greivenkamp. *Field Guide to Geometrical Optics*. Field Guide Series. SPIE Press, 2004.